

# Self-Supervised Learning-Based Path Planning and Obstacle Avoidance Using PPO and B-Splines in Unknown Environments

Shahab Shokouhi

*Department of Mechanical Engineering  
University of New Hampshire  
Durham, New Hampshire, USA  
shahaab.shokouhi@unh.edu*

Oguzhan Oruc

*Department of Mechanical Engineering  
The Citadel School of Engineering  
Charleston County, South Carolina, USA  
ooruc@citadel.edu*

May-Win Thein

*Department of Mechanical Engineering  
University of New Hampshire  
Durham, New Hampshire, USA  
may-win.thein@unh.edu*

**Abstract**—This paper introduces SmartBSP, an advanced self-supervised learning framework for real-time path planning and obstacle avoidance in autonomous robotics navigating through complex environments. The proposed system integrates Proximal Policy Optimization (PPO) with Convolutional Neural Networks (CNN) and Actor-Critic architecture to process limited LIDAR inputs and compute spatial decision-making probabilities. The robot's perceptual field is discretized into a grid format, which the CNN analyzes to produce a spatial probability distribution. During the training process a nuanced cost function is minimized that accounts for path curvature, endpoint proximity, and obstacle avoidance. Simulations results in different scenarios validate the algorithm's resilience and adaptability across diverse operational scenarios. Subsequently, Real-time experiments, employing the Robot Operating System (ROS), were carried out to assess the efficacy of the proposed algorithm.

**Index Terms**—Real-time Path Planning, Convolutional Neural Network, B-spline, Self-Supervised Learning, Proximal Policy Optimization

## I. INTRODUCTION

Autonomous navigation and environment mapping for autonomous vehicles has garnered considerable attention in the field of robotics and autonomous systems research [1] [2]. More specifically, path planning methodologies are divided into two primary categories: one focusing on navigation within entirely unknown environments [3], where we only have access to real-time range sensor data, and the other dedicated to environments that are either partially or completely known [4]. The interest in path planning in unknown environments is driven by the critical need for autonomous vehicles to operate effectively in situations where prior knowledge of the environment is absent or severely limited. Examples of such applications include extraterrestrial rover missions on planets like Mars, where the terrain is largely uncharted, and search-and-rescue operations in disaster-stricken areas, where rapid changes in the environment preclude the use of pre-existing maps.

Additionally, the advent of Artificial Intelligence (AI) has revolutionized the way researchers tackle the path planning problem [5], [6]. By harnessing the power of AI, scholars are now able to construct neural networks that not only learn from

simulated and real data but also exhibit human-like expertise in decision-making processes [7]. However, the lack of access to useful data makes training neural networks offline for path planning challenging. In such situations, self-supervised learning methods have proven to be effective [8]. Nevertheless, learning on real-time experimental data can be time-consuming and sometimes unsafe [9]. To ensure safe learning, Proximal Policy Optimization (PPO) [10] has been employed to train the path planner offline. While PPO is widely known as a method in Reinforcement Learning (RL), its application in this paper is slightly different. This study assumes that there is no transition between states (observations), meaning the impact of decisions made at any time step on future events is ignored.

While the safety of the path plays a major role in the path planning task, the smoothness of the path is equally important. Due to the low maneuverability of some vehicles, paths with high curvature or sudden changes in yaw angle are not feasible. In recent years, B-splines have been employed in numerous studies to minimize the curvature of the path [11]–[13]. While these studies have made notable advancements in incorporating curvature and smoothness into path planning, the computational demand and possible numerical instability of their methods—especially when dealing with non-convex obstacles—present significant challenges for real-time implementation.

The method proposed in this paper incrementally builds the path based on new information received from the LIDAR sensor. The main objective of the algorithm is to find the optimal positions of control points for a local B-spline that guides the vehicle toward the target while avoiding obstacles and minimizing curvature. The contributions of this paper to the field of path planning include the following:

- The proposed path planning algorithm is tailored for completely unknown environments, capable of overcoming various non-convex obstacles.
- The method introduced here explicitly incorporates path smoothness.

- The algorithm is designed for rapid execution, enabling real-time path planning.
- The algorithm is generalizable to different vehicles and environments by adjusting its hyperparameters, such as field of view and range.
- The position of the target location is generalized, meaning there is no need to train the path planner for each different target location.

The remainder of the paper is structured as follows: Section II reviews related work, providing an overview of existing AI-based path planning methodologies and their limitations. Section III delves into the methodology, detailing the various components involved in the SmartBSP algorithm, including the integration of Proximal Policy Optimization (PPO) with Convolutional Neural Networks (CNNs) and the Actor-Critic architecture. Section IV discusses the simulation results, highlighting the performance of the SmartBSP algorithm across different scenarios and the parameters used in the simulations. Section V focuses on the experimental results, showcasing the practical implementation and testing of the SmartBSP algorithm on a real-world robotic platform. The conclusion summarizes the findings and outlines potential directions for future research.

## II. RELATED WORK

In recent years, deep learning algorithms have been used in many studies to enhance traditional path planning methods. For example, in [14], Convolutional Neural Networks (CNNs) are employed to learn pre-planned paths from other offline path planning methods, marking a significant step towards leveraging image-based methodologies in path planning. In [5], Double Deep Q-Learning is utilized to navigate path planning challenges within dynamically changing environments. Sharma et al. [6] have employed Q-learning techniques to determine the optimal path in a known environment, with the specific limitation that the goal's location is not generalized across different scenarios. In [15], Deep Q-learning and CNNs are utilized to construct paths within grid patches derived from the environment. Wang et al. [16] leveraged neural networks to improve the probability distribution of sampling in Rapidly-exploring Random Trees Star (*RRT\**) algorithm, aiming to accelerate the convergence towards an optimal solution. Pflueger et al. [8] proposed an approach using inverse reinforcement learning with soft value iteration networks (SVIN) for planetary rover path planning. This method leverages deep convolutional networks and value iteration networks to handle the complexities of navigation on Mars, demonstrating its effectiveness on both grid world and realistic Mars terrain datasets. Chiang et al. [17] introduced RL-RRT, a kinodynamic motion planner that combines reinforcement learning with sampling-based planning. Their method uses deep reinforcement learning to train an obstacle-avoiding policy, which serves as a local planner, and a reachability estimator that predicts the time to reach a state in the presence of obstacles. The next section describes the methodology and steps involved in our proposed method.

## III. METHODOLOGY

The primary objective of the proposed path planning is finding the optimal control points of B-splines, similar to [11], but diverges from the author's previous works by integrating a novel approach that serves two purposes: 1) it accelerates the optimization process in real-time and 2) it is capable of addressing many non-convex obstacles in the environment. Central to this methodology is the consideration of both curvature and the spatial distance of the final point of each local B-spline to the target, while concurrently ensuring avoidance of detected obstacles within the sensor range.

Distinctive to this study is the initial transformation of the perceived point cloud into an  $n \times n$  circular grid representation, which is depicted in Fig. 1 (a). Grid cells that have more than  $m$  points are considered as obstacles. In this paper, a  $5 \times 5$  grid configuration has been employed, comprising 5 angular intervals and 5 radial intervals. The transformation emulates the configuration of contemporary range sensors commonly deployed in autonomous vehicle platforms. This preprocessing step enhances the method's applicability, rendering it more congruent with real-world scenarios.

Subsequently, the circular grid undergoes a conversion process to a square grid format (Fig. 1 (b)). This conversion facilitates seamless integration with a convolutional neural network (CNN), a pivotal component of the proposed methodology. The CNN operates on the square grid input and outputs the probability distribution governing the selection of each control point for the B-spline trajectory. Notably, it is imperative to acknowledge that within this transformation framework, the angular coordinate of the circular grid corresponds to the  $y$  coordinates in the square coordinate system, whereas the radial coordinate aligns with the  $x$  coordinates. The rest of this section explains the main components of the proposed method.

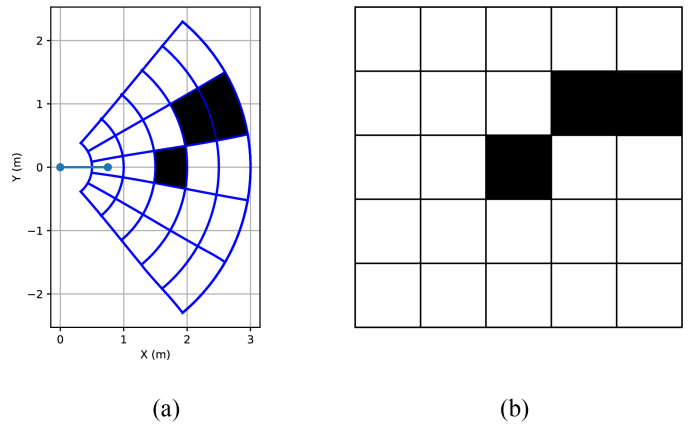


Fig. 1. (a) Circular grid formed based on observed point cloud, (b) equivalent square grid

### A. Environment

In the context of an self-supervised learning problem, the environment serves as a component that processes inputs or

actions alongside current states, yielding subsequent rewards or costs. Formally, we define the environment as  $\mathcal{E} = (C, \mathcal{S})$ , where  $\mathcal{S}$  represents the observed point cloud (state) and  $C$  signifies the cost function. It is noteworthy that the choice between reward maximization and cost minimization is arbitrary, as maximizing reward can be equivalently framed as minimizing cost. Additionally, it is assumed that there is no transition between states, meaning that the learning problem focuses on improving the outcome by adjusting the actions (control points of the B-spline) for each given  $5 \times 5$  grid configuration.

The radial coordinates of the control points are predetermined, comprising  $n + 1$  radial coordinates incrementally increasing from zero to the sensor range, inclusive of the origin which signifies the location of the robot at each time step. Since the location of the first and second control points is predetermined, as shown in Fig. 1 (a), the learning algorithm is assigned the responsibility of choosing among  $n - 1$  distinct angular coordinates (actions) for the remaining control points. The first and second control points are always at fixed positions relative to the robot to mitigate abrupt changes in the desired yaw angle. Therefore, the set of all control points (actions)  $\mathcal{A}$  can be written as:

$$\mathcal{A} = \{\mathcal{A}_1, \mathcal{A}_2, \dots, \mathcal{A}_{n+1}\}$$

Control points  $\mathcal{A}_3, \dots, \mathcal{A}_{n+1}$  are the geometric centers of the chosen cell grids. Given  $\mathcal{A}$ , the cost of the B-spline can be calculated using the following formula:

$$C(\mathcal{S}, \mathcal{A}) = \rho_1 C_{\text{dist}} + \rho_2 C_{\text{curv}} + \rho_3 C_{\text{obs}} \quad (1)$$

In this equation,  $\rho_i$ , where  $i = 1, 2, 3$ , are the weights,  $C_{\text{dist}}$  represents the cost imposed due to the L2 norm between the final point of the B-spline and the final target:

$$C_{\text{dist}}(\mathcal{A}) = \|\mathcal{A}_{n+1} - \mathcal{G}_{\text{final}}\|_2 \quad (2)$$

where  $\mathcal{G}_{\text{final}}$  is the target location in  $xy$ -plane. The term  $C_{\text{curv}}$  denotes the cost imposed by the overall curvature of the B-spline, and  $C_{\text{obs}}$  denotes the cost imposed due to collision with obstacles. In this paper, we define the cost imposed by the overall curvature of B-spline as

$$C_{\text{curv}}(\mathcal{A}) = \int_{\mathcal{A}_1}^{\mathcal{A}_{n+1}} k(\beta)^2 d\beta \quad (3)$$

where  $\beta$  is any point on the B-spline and  $k(\beta)$  is defined at each point as

$$k(\beta) = \frac{y''(\beta)}{(1 + y'(\beta)^2)^{3/2}} \quad (4)$$

Note that all the derivatives in (4) are with respect to  $\beta$ . Furthermore,  $C_{\text{obs}}$  is

$$C_{\text{obs}}(\mathcal{S}, \mathcal{A}) = \begin{cases} 1 & \text{if collision = TRUE} \\ 0 & \text{otherwise} \end{cases} \quad (5)$$

## B. Proximal Policy Optimization

Before delving into the intricacies of Proximal Policy Optimization (PPO) [10], the framework of the self-supervised learning problem can be established as follows:  $(\mathcal{S}, \mathcal{A}, C)$  is defined where  $\mathcal{S}$  denotes the current state, representing the observed circle segment captured by the range sensor;  $\mathcal{A} = (\mathcal{A}_1, \dots, \mathcal{A}_{n+1})$  represents the set of  $n + 1$  actions, i.e., control points, selected at the current state;  $C$  signifies the cost associated with choosing  $\mathcal{A}$  at  $\mathcal{S}$ , calculated via (1). Note that each  $\mathcal{A}_i$ ,  $i = 3, \dots, n + 1$ , is sampled from a discrete distribution over  $n$  possible outcomes.

PPO can be characterized as a learning method that learns by increasing the probability of selecting actions that outperform the average. The primary distinction between PPO and other reinforcement learning methods is its endeavor to restrict the steps taken in gradient descent to mitigate the risk of local optima. PPO revolutionizes policy optimization by introducing two pivotal innovations: the Clipped Surrogate Objective (CSO) and the utilization of multiple epochs of stochastic gradient ascent for each policy update. Here, the policy is defined as

$$\pi_{\theta}(a|\mathcal{S}) = P(\mathcal{A} = a|\mathcal{S}) \quad (6)$$

where  $\theta$  are the parameters of the neural network and  $a$  is the sampled action vector. Since each B-spline consists of  $n - 1$  different actions plus the first and second points, which are fixed, the probability of choosing each specific B-spline or path is as follows:

$$\pi_{\theta}(a|\mathcal{S}) = \prod_{i=3}^{n+1} \pi_{\theta}(a_i|\mathcal{S}) \quad (7)$$

or in the *log* form

$$\log \pi_{\theta}(a|\mathcal{S}) = \sum_{i=3}^{n+1} \log \pi_{\theta}(a_i|\mathcal{S}) \quad (8)$$

PPO utilizes the ratio of the probability to constrain the policy update. The ratio is defined as

$$r(\theta) = \frac{\pi(a|\mathcal{S})}{\pi_{\text{old}}(a|\mathcal{S})}$$

This is achieved through CSO function:

$$L^{\text{clip}}(\theta) = \hat{\mathbb{E}}[\min(r(\theta)\hat{A}, \text{clip}(r(\theta), 1 - \epsilon, 1 + \epsilon)\hat{A})] \quad (9)$$

Here, the hyperparameter  $\epsilon$  is typically set to a specific value, for instance,  $\epsilon = 0.2$  [10], and  $\hat{A}$  represents the advantage function, distinct from the action vector  $\mathcal{A}$ :

$$\hat{A} = C(\mathcal{S}, a) - \mathbb{E}_{a \in \mathcal{A}}[C(\mathcal{S}, a)] \quad (10)$$

Note that  $r(\theta)$  exceeds 1 when the action is more probable for the current policy than for the old policy; it will range between 0 and 1 when the action is less probable for the current policy than for the old one. The advantage function evaluates the quality of the sampled actions relative to the expected cost, which should be estimated using the critic

network, as explained in the following subsection. To clarify, when the cost of the sampled path exceeds the expected cost, the advantage function is positive. Consequently, to minimize (9), the probability of that action vector should decrease in the new update. Conversely, when the cost of the sampled path is lower than the expected cost, the advantage function is negative. Thus, to minimize (9),  $r_t(\theta)$  should increase. Furthermore, the *clip* function constrains the update ratio  $r_t(\theta)$  within the interval  $[1 - \epsilon, 1 + \epsilon]$ , thereby preventing large steps from being taken.

### C. Actor-Critic Architecture

The dual-component setup of actor-critic architecture enables it to efficiently learn complex policies in environments with high-dimensional state and action spaces, making it well-suited for a wide range of learning tasks. The overall configuration of the AC architecture used in this paper is shown in Fig. 2.

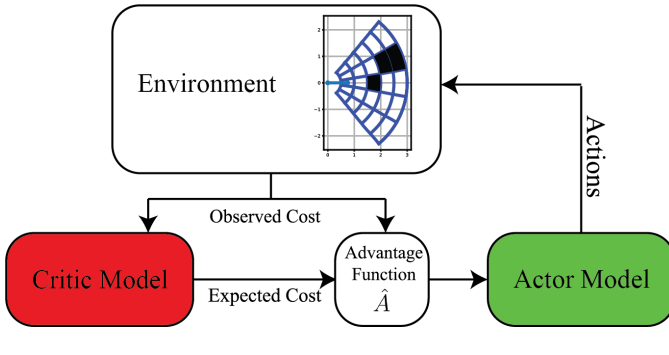


Fig. 2. Actor-Critic architecture

In this paper, the authors have employed two simple CNNs to learn the policy and the expected cost at each observation, represented by a  $5 \times 5$  grid occupied by obstacles. Fig. 3 depicts the schematic of the architecture used as actor. The output of the actor network is a  $5 \times 5$  matrix. Then, each column of the output is passed through a softmax function to convert it to a probability distribution. The selected action at each column is sampled from this probability distribution. It is worth noting that the distribution obtained from the first column of the output is irrelevant since the first column corresponds to the second point of the B-spline, which is predetermined. On the other hand, the critic part takes the  $5 \times 5$  matrix as input and estimates the baseline, or the expected cost, to calculate the advantage function. The configurations of the critic network is represented in Fig. 4. The loss function used to update the weights of the critic network is Mean Squared Error function:

$$\text{MSE}(C, \hat{C}) = \frac{1}{l} \sum_{i=1}^l (C_i - \hat{C}_i)^2 \quad (11)$$

where  $l$  is the batch size, and  $\hat{C}$  is the estimated cost.

### D. Target Generalization

One of the primary challenges encountered when applying CNN-based methods for path planning tasks is the incorpora-

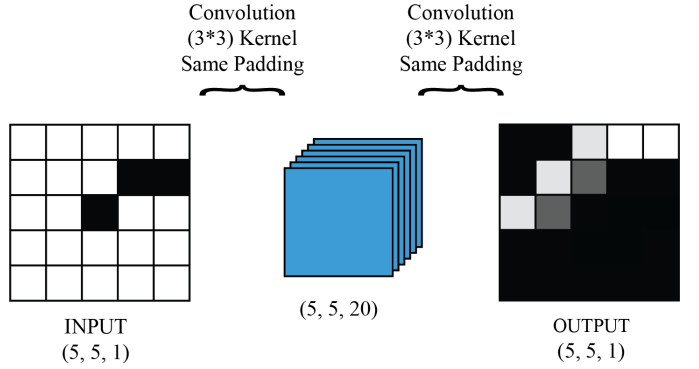


Fig. 3. Actor network architecture

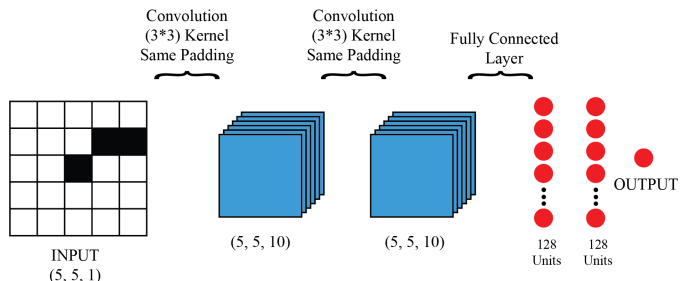


Fig. 4. Critic network architecture

tion of the target location into the network. Due to the limited field of view of the robot, achieving a globally optimized solution is not feasible. However, akin to how humans confront this dilemma in real-life scenarios, the robot selects a goal location within its field of view. In this approach, we calculate the distance between the final target and all five potential final points of the B-spline. Subsequently, we select the point closest to the final target, referred to as the normalized target in this study (Fig. 5). The set containing all five normalized targets is:

$$\mathcal{G} = \{\mathcal{G}_1, \mathcal{G}_2, \dots, \mathcal{G}_5\}$$

and the final target is denoted as  $\mathcal{G}_{\text{final}}$ .

Moreover, we train five distinct actor networks, each targeting a different potential normalized target. In other words, the  $C_{\text{dist}}$  component of (1) represents the distance between the final point of the path and the normalized target. Subsequently, the network associated with the normalized target suggests a path. However, when the path to the normalized target location is obstructed, the actor fails to propose a collision-free path. In such instances, we assume that the robot has encountered either a wall or a non-convex obstacle. Although the proposed method does not offer a path for all non-convex obstacles, to address such scenarios, we shift the normalized target from the closest one to the final target to the one with the minimum cost calculated by

$$C_i(\mathcal{S}, \mathcal{A}) = \rho_2 C_{\text{curv}} + \rho_3 C_{\text{obs}} \quad (12)$$

referred to as the temporary target  $\mathcal{G}_{\text{temp}}$ . Here,  $C_i, i =$

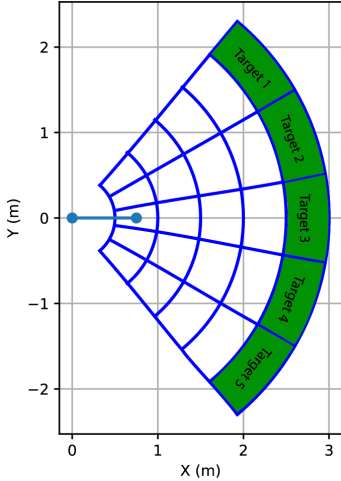


Fig. 5. Five potential temporary goal locations

$1, \dots, n$ , represents the cost associated with normalized target  $i$  as shown in Fig. 5. Note that the set of control points associated with  $\mathcal{G}_{\text{temp}}$ , is denoted by  $\mathcal{A}_{\text{temp}}$ . This adjustment will continue until the normalized target is no longer obstructed. Situations where even this adjustment of the goal fails can be categorized into two different types: (1) when all the temporary targets are obstructed, a rare occurrence, particularly when the path update rate is high or the field of view is wide, and (2) when we encounter extreme non-convexities, such as U-shaped obstacles. Here, the authors assume that none of these situations would occur.

TABLE I  
TRAINING PARAMETERS

Parameter	Value
batch size	10
# of epochs	3
learning rate	0.001
$\epsilon$ (PPO clipping constant)	0.2
# of updates per iteration	5

#### IV. SIMULATION RESULTS

To train each of the five aforementioned networks, 10,000  $5 \times 5$  grid samples with randomly distributed obstacles are generated. The training hyperparameters are presented in Table I.

Table II represents the success rates of the trained networks. Here, success is defined as the ability to avoid all obstacles present in the local grid.

It is needless to say that since grids are occupied by ones and zeros, causing symmetries to occur in many samples, choosing the appropriate seed plays an important role in the success rate of trained networks.

TABLE II  
SUCCESS RATE OF TRAINED NETWORKS

Trained Neural Networks	Success Rate
NN 1	96%
NN 2	95%
NN 3	95%
NN 4	95%
NN 5	97%

#### Algorithm 1 SmartBSP Algorithm

---

```

while target position is not reached do
    Acquire sensor data  $\mathcal{S}$  using the LIDAR sensor
    Update the local occupancy grid with observed points
    if  $\mathcal{S} \neq \emptyset$  then
        Calculate the coordinates of the normalized targets
        Choose the network associated with the closest target
        Generate  $\mathcal{A} \Rightarrow$  Calculate  $C(\mathcal{S}, \mathcal{A})$ 
        if  $C_{\text{obs}}(\mathcal{S}, \mathcal{A}) = 1$  then
             $\mathcal{G}_{\text{temp}} = \mathcal{G}_i$  where  $i = \underset{i \in \{1, 2, \dots, n\}}{\text{argmin}} C_i(\mathcal{S}, \mathcal{A})$ 
            Generate  $\mathcal{A}_{\text{temp}}$ 
        end if
    else
         $\mathcal{G} = \mathcal{G}_{\text{final}}$ 
    end if
    Follow 10% of the planned path segment.
end while

```

---

The steps followed in simulation and experimental sections are summarized in Algorithm 1. Depending on the complexity of the environment, one can adjust the path update rate. In environments with numerous obstacles, the path should be updated more frequently. In this study, the path is updated when 10% of the path is traversed. The chosen vehicle for the simulation is a simple differential drive robot, which utilizes a PID controller to follow the path. The robot and the sensor parameters are represented in Table III. The PID controller coefficients are adjusted to minimize tracking error. It is essential to note that the controller can have a significant impact on the path planner's functionality. Therefore, using a well-designed controller is vital.

TABLE III  
THE DIFFERENTIAL DRIVE ROBOT AND RANGE SENSOR PARAMETERS

Parameter	Value
Wheelbase	0.15 m
Wheel Radius	0.05 m
Sensor Range	3 m
Field of View	100 deg
Radial Intervals	0.5 m
Angular Intervals	20 deg

To demonstrate the capabilities of the proposed algorithm,

various scenarios are tested against the path planner. The obstacles' edges in each scenario are represented by points to simulate feedback from conventional range sensors. Notably, the environment itself is not divided into grid cells. When the vehicle seeks to update its path at any given time step, it observes the circular segment ahead of it. Each circular grid cell containing a certain number of points is then marked as an obstacle. The output of this process is depicted in Fig. 1(b).

#### A. Scenario 1: Environments with multiple small obstacles

In this scenario, the environment is populated with obstacles of uniform size, randomly positioned throughout. The vehicle starts from the origin and navigates towards the target piece by piece, relying on its limited field of view. The simulation concludes when the robot's distance to the target is less than 3 m. Fig. 6 illustrates how the robot can overcome non-convex obstacles. It is important to note that the level of non-convexity significantly impacts the algorithm's performance. Specifically, if addressing non-convex situations requires information on past observed environments and decisions, the algorithm may fail. However, the authors have only utilized environments lacking such complexities.

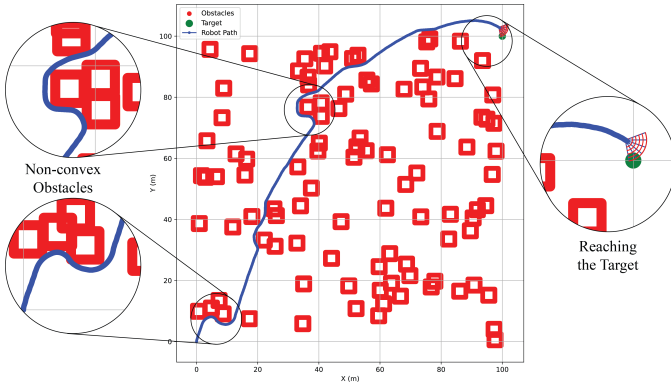


Fig. 6. Path planning result in scenario 1

#### B. Scenario 2: Passing wall-like obstacles

Passing a wall-like obstacle without knowledge of its endpoint poses a significant challenge. When the vehicle encounters the wall, it must decide whether to turn right or left. Given the limited field of view, making an optimal decision regarding the distance traveled by the vehicle becomes impossible. Here, the assumption is made that the wall is short, meaning that turning right or left would not significantly impact the solution. Fig. 7 illustrates the performance of the algorithm in such scenarios.

#### V. EXPERIMENTAL RESULTS

To test the algorithm performance in real situations, the Jettracer platform has been employed. The JetRacer robot, shown in Fig. 8, is a small-scale, autonomous vehicle designed for experimentation and research purposes. Equipped with a variety of sensors and a Jetson Nano onboard computer, the

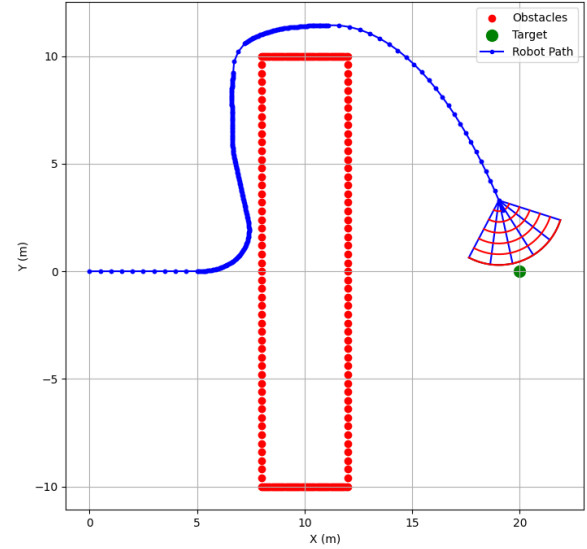


Fig. 7. Path planning result in scenario 2

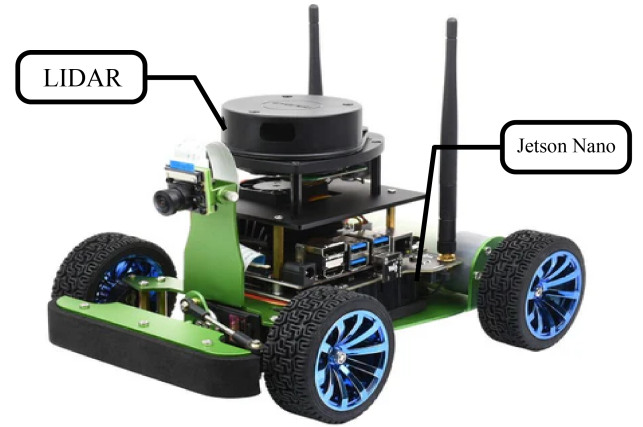


Fig. 8. Jetracer platform

JetRacer is capable of executing complex navigation tasks in dynamic environments.

To estimate its location, the JetRacer utilizes a combination of an Inertial Measurement Unit (IMU) and wheel odometry, which provides sufficient precision for the purposes outlined in this paper. The estimated location is then passed through an Extended Kalman Filter to reduce noise and increase the accuracy of odometry. Additionally, the JetRacer platform is equipped with a 360° LIDAR sensor to detect obstacles. The LIDAR range is 12m, but to mimic the algorithm used in

this paper, the output of the LIDAR is filtered to limit the range and the field of view. It is important to note that the selection of these parameters, such as the range and field of view of the LIDAR sensor, depends on the maneuverability of the robot and the number and shape of obstacles present in the environment.

To maintain the desired path, a straightforward PID controller is utilized. The controller gains are fine-tuned through trial and error to minimize tracking errors. The vehicle maintains a constant forward speed, while the controller dynamically adjusts the steering angle based on the next waypoint provided by the path planner. Fig. 9 illustrates the interconnectedness of various components of the platform through the Robot Operating System (ROS). The entire system is designed with modularity in mind, facilitating easy replacement of the controller and path planner for future research endeavors.

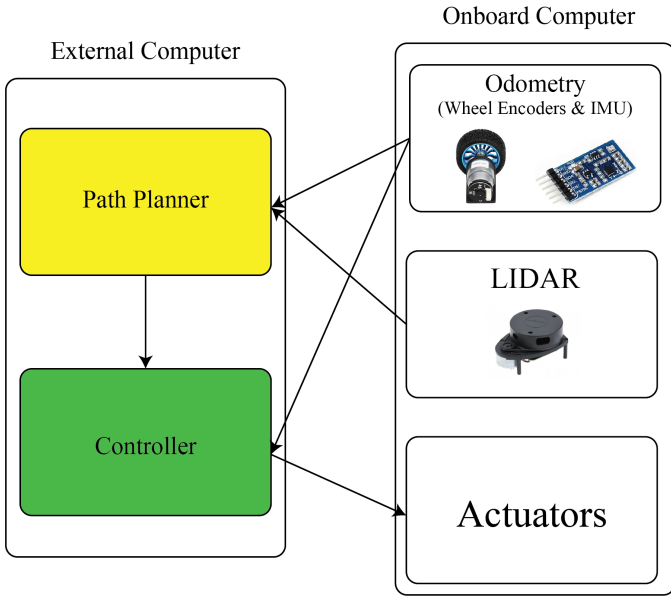


Fig. 9. ROS modules configuration

To assess the algorithm, the vehicle is tested in two different scenarios. Fig. 10 and Fig. 11 present the results of the first test. The final goal is located behind a wall, requiring the robot to circumvent a non-convex wall to reach it. To perform this test, the vehicle's field of view is set to  $120^\circ$  and the sensor range to 0.8 m. It is important to note that the robot has no prior knowledge of the environment. The starting position, denoted by yellow, is considered the origin. The robot is programmed to stop when it is within a predefined distance from the target position. The red points represent the observations made by the LIDAR sensor during the tests. The entire path is planned incrementally, utilizing the robot's limited field of view.

In the second test, the robot is subjected to a more complex situation. Fig. 12 and Fig. 13 illustrate the results of the second test. During the test, it was observed that the field of view plays a crucial role in the vehicle's success rate. To overcome this test, the robot required a field of view of  $180^\circ$ . It should

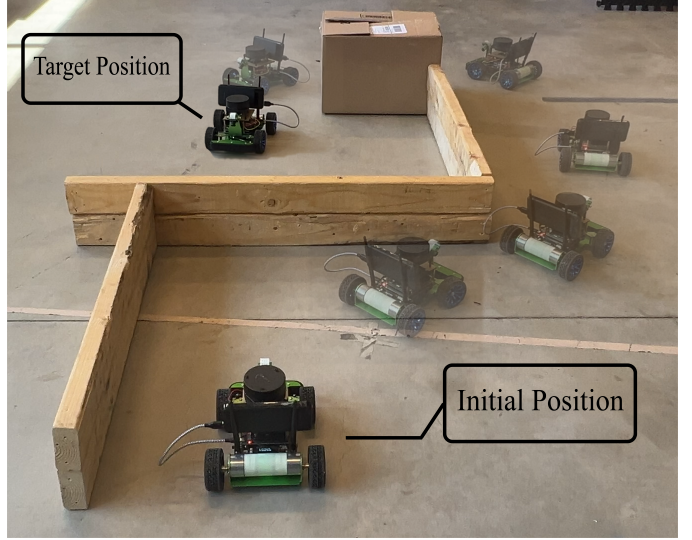


Fig. 10. Test 1: Reaching Targets Located Behind a Wall-Shaped Obstacle

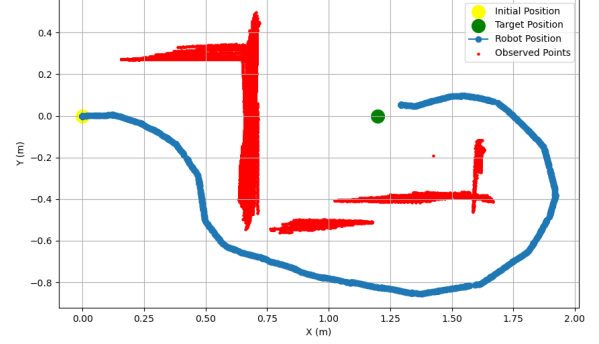


Fig. 11. Test 1: Robot Path and Observed Environment

be noted that changing the field of view is achieved simply by adjusting the filter on the LIDAR sensor, without the need to retrain the networks. In other words, the proposed method is generalizable to different environments by fine-tuning the sensor range and field of view.

## VI. CONCLUSION

In this paper, we introduced SmartBSP, an AI-based path planning approach designed for autonomous robotics in complex and unknown environments. By leveraging Proximal Policy Optimization (PPO) combined with Convolutional Neural Networks (CNNs) and an Actor-Critic architecture, our method effectively processes limited LIDAR inputs to generate optimal paths in real-time. The integration of B-spline curves and a nuanced cost function accounting for path curvature, endpoint proximity, and obstacle avoidance further enhances the robustness and adaptability of the system.

Through extensive simulations and real-world experiments, we demonstrated that the proposed method can handle various challenging scenarios, including environments with multiple

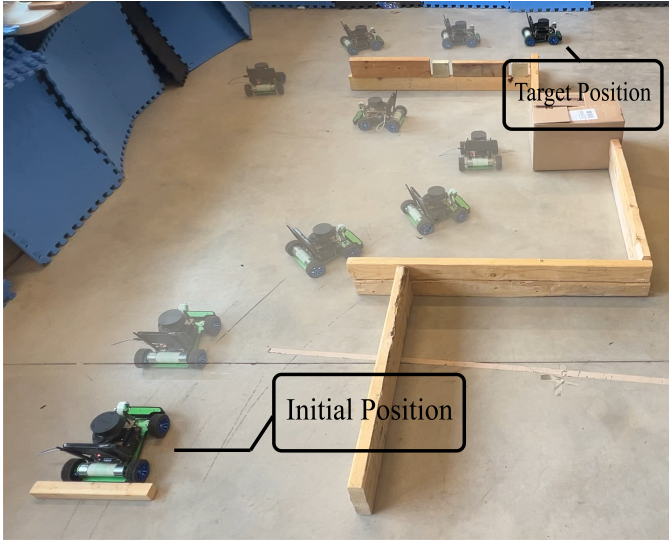


Fig. 12. Test 2: Robot Path and Observed Environment

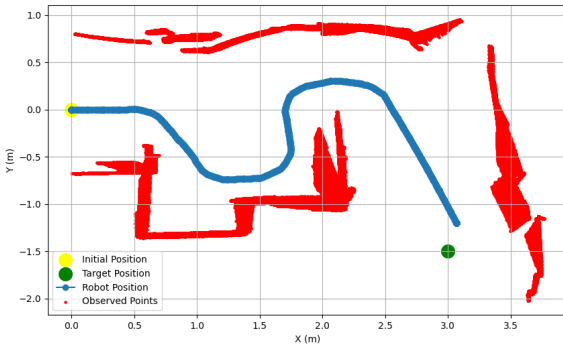


Fig. 13. Test 2: Robot Path and Observed Environment

small obstacles and wall-like obstacles. Our results show that adjusting the field of view and sensor range significantly impacts the success rate of the vehicle, highlighting the importance of these parameters in path planning tasks. Moreover, the flexibility of the SmartBSP approach allows for easy adaptation to different environments without the need for retraining the networks, showcasing its potential for practical applications in diverse operational scenarios.

Future work will focus on further refining the algorithm to handle more complex non-convex obstacles and exploring the integration of additional sensor modalities to enhance the perception capabilities of the autonomous system. Additionally, we aim to apply the SmartBSP framework to other types of autonomous vehicles and investigate its performance in large-scale outdoor environments.

## REFERENCES

- [1] A. M. Wyglinski et al., "Phantom Car Attack Detection via Passive Opportunistic RF Localization," in *IEEE Access*, vol. 11, pp. 27676-27692, 2023.
- [2] Sánchez-Ibáñez, J.R.; Pérez-del-Pulgar, C.J.; García-Cerezo, A. Path Planning for Autonomous Mobile Robots: A Review. *Sensors* 2021, 21.
- [3] W. Khaksar, S. Vivekananthen, K. S. M. Saharia, M. Yousefi and F. B. Ismail, "A review on mobile robots motion path planning in unknown environments," 2015 IEEE International Symposium on Robotics and Intelligent Sensors (IRIS), Langkawi, Malaysia, 2015, pp. 295-300.
- [4] Raja, Purushothaman, and Sivagurunathan Pugazhenthi. "Optimal path planning of mobile robots: A review." *International journal of physical sciences* 7.9 (2012): 1314-1320.
- [5] Xiaoyun Lei, Zhian Zhang, Peifang Dong, "Dynamic Path Planning of Unknown Environment Based on Deep Reinforcement Learning", *Journal of Robotics*, vol. 2018, Article ID 5781591, 10 pages, 2018.
- [6] A. Sharma, K. Gupta, A. Kumar, A. Sharma and R. Kumar, "Model based path planning using Q-Learning," 2017 IEEE International Conference on Industrial Technology (ICIT), Toronto, ON, Canada, 2017, pp. 837-842.
- [7] S. R. Ravigopal, T. A. Brumfiel, A. Sarma and J. P. Desai, "Fluoroscopic Image-Based 3-D Environment Reconstruction and Automated Path Planning for a Robotically Steerable Guidewire," in *IEEE Robotics and Automation Letters*, vol. 7, no. 4, pp. 11918-11925, Oct. 2022.
- [8] M. Pflueger, A. Agha and G. S. Sukhatme, "Rover-IRL: Inverse Reinforcement Learning With Soft Value Iteration Networks for Planetary Rover Path Planning," in *IEEE Robotics and Automation Letters*, vol. 4, no. 2, pp. 1387-1394, April 2019.
- [9] R. Szczepanski, "Safe Artificial Potential Field - Novel Local Path Planning Algorithm Maintaining Safe Distance From Obstacles," in *IEEE Robotics and Automation Letters*, vol. 8, no. 8, pp. 4823-4830, Aug. 2023.
- [10] Schulman J, Wolski F, Dhariwal P, Radford A, Klimov O. Proximal policy optimization algorithms. *arXiv preprint arXiv:1707.06347*. 2017 Jul 20.
- [11] S. Shokouhi, B. Mu and M. -W. Thein, "Optimized Path Planning and Control for Autonomous Surface Vehicles using B-Splines and Nonlinear Model Predictive Control," *OCEANS 2023 - MTS/IEEE U.S. Gulf Coast, Biloxi, MS, USA*, 2023, pp. 1-9.
- [12] C. Shen, Y. Shi and B. Buckingham, "Integrated Path Planning and Tracking Control of an AUV: A Unified Receding Horizon Optimization Approach," *IEEE/ASME Transactions on Mechatronics*, vol. 22, no. 3, pp. 1163-1173, June 2017.
- [13] Sabiha, A.D., Kamel, M.A., Said, E. et al. Real-time path planning for autonomous vehicle based on teaching-learning-based optimization. *Intel Serv Robotics* 15, 381-398 (2022).
- [14] D. Sartori, D. Zou, L. Pei and W. Yu, "CNN-based path planning on a map," 2021 IEEE International Conference on Robotics and Biomimetics (ROBIO), Sanya, China, 2021, pp. 1331-1338.
- [15] Aleksandr I. Panov, Konstantin S. Yakovlev, Roman Suvorov, "Grid Path Planning with Deep Reinforcement Learning: Preliminary Results", *Procedia Computer Science*, Volume 123, 2018, Pages 347-353, ISSN 1877-0509,
- [16] J. Wang, W. Chi, C. Li, C. Wang and M. Q. . -H. Meng, "Neural RRT\*: Learning-Based Optimal Path Planning," in *IEEE Transactions on Automation Science and Engineering*, vol. 17, no. 4, pp. 1748-1758, Oct. 2020
- [17] H. -T. L. Chiang, J. Hsu, M. Fiser, L. Tapia and A. Faust, "RL-RRT: Kinodynamic Motion Planning via Learning Reachability Estimators From RL Policies," in *IEEE Robotics and Automation Letters*, vol. 4, no. 4, pp. 4298-4305, Oct. 2019.